2018

Importance of hydrothermal vents in scavenging removal of 230Th in the Nansen Basin

O. Valk

M. M. Rutgers van der Loeff

W. Geibert

S. Gdaniec

M. J.A. Rijkenberg

See next page for additional authors

Authors

O. Valk, M. M. Rutgers van der Loeff, W. Geibert, S. Gdaniec, M. J.A. Rijkenberg, S. B. Moran, K. Lepore, R. L. Edwards, Y. Lu, and Viena Puigcorbe

Importance of Hydrothermal Vents in Scavenging Removal of ^{230}Th in the Nansen Basin

O. Valk[1] (ID), M. M. Rutgers van der Loeff[1] (ID), W. Geibert[1] (ID), S. Gdaniec[2] (ID), M. J. A. Rijkenberg[3,4], S. B. Moran[5] (ID), K. Lepore[6], R. L. Edwards[7], Y. Lu[8], and V. Puigcorbé[9] (ID)

[1]Alfred Wegener Institute, Helmholtz Centre for Polar and Marine Research, Bremerhaven, Germany, [2]Department of Geological Sciences, Stockholm University, Stockholm, Sweden, [3]Department of Ocean Systems, NIOZ Royal Institute for Sea Research, Den Burg, The Netherlands, [4]Utrecht University, Utrecht, The Netherlands, [5]College of Fisheries and Ocean Sciences, University of Alaska Fairbanks, Fairbanks, AK, USA, [6]Mount Holyoke College, South Hadley, MA, USA, [7]Department of Earth Sciences, University of Minnesota, Minneapolis, MN, USA, [8]Earth Observatory of Singapore, Climate, Nanyang Technological University, Singapore, [9]School of Science, Edith Cowan University, Joondalup, WA, Australia

Abstract In this study we present dissolved and particulate ^{230}Th and ^{232}Th results, as well as particulate ^{234}Th data, obtained as part of the GEOTRACES central Arctic Ocean sections GN04 (2015) and IPY11 (2007). Samples were analyzed following GEOTRACES methods and compared to previous results from 1991. We observe significant decreases in ^{230}Th concentrations in the deep waters of the Nansen Basin. We ascribe this nonsteady state removal process to a variable release and scavenging of trace metals near an ultraslow spreading ridge. This finding demonstrates that hydrothermal scavenging in the deep-sea may vary on annual time scales and highlights the importance of repeated GEOTRACES sections.

Plain Language Summary This study presents new results of thorium isotopes from the central Arctic Ocean. Thorium-230 is produced continuously in seawater by radioactive decay of ^{234}U and subsequently removed by particle scavenging. We show that observed changes in ^{230}Th concentrations compared to earlier times are related to submarine volcanic eruptions. We use ^{230}Th data from three different expeditions conducted in 1991, 2007, and 2015. The Nansen Basin is part of the Eurasian Basin of the Arctic Ocean. It is divided from the Amundsen Basin by the Gakkel Ridge. The Gakkel Ridge is a region where the Eurasian and the North American plates spread apart, triggering volcanism. Submarine volcanos and hydrothermal vents release trace elements such as iron. Iron is known to be oxidized to particles that react with ^{230}Th. Thus, when iron particles sink they remove ^{230}Th from the water column. In the Nansen Basin this process took place between 2007 and 2015, triggered by earthquake-induced volcanic eruptions in 2001. In this study, we present a conceptual hydrothermal scavenging process and plume dispersal by deep water circulation.

1. Introduction

^{230}Th ($t_{1/2}$ = 75,690 years) is produced in the ocean by the radioactive decay of dissolved ^{234}U and removed from the water column by scavenging onto sinking particles (Bacon & Anderson, 1982). Its water column distribution is the result of scavenging, circulation, and in-growth (Henderson et al., 1999; Scholten et al., 1995). ^{232}Th ($t_{1/2}$ = 1.4 × 10^{10} years) in seawater is supplied by lithogenic materials (Santschi et al., 2006). Thorium isotopes are widely used tracers for particle fluxes and water mass advection (Coppola et al., 2006; Roy-Barman et al., 2002).

A recent study shows the importance of hydrothermal activity in Th removal in the South East Pacific (Pavia et al., 2017). Hydrothermal plumes are sources of many trace elements, for example, Fe and Mn (Klinkhammer et al., 1977; Resing et al., 2015; Saito et al., 2013) and sinks for others, including Th, due to scavenging onto particles or mineral coprecipitation (German et al., 1991, 2002). Hydrothermal particulate Fe scavenges ^{230}Th (Hayes et al., 2015). Hydrothermal plumes can travel over large distances (Fitzsimmons et al., 2014) and can cause ^{230}Th deficits even several thousand kilometers off axis (Pavia et al., 2017).

The ultraslow spreading Gakkel Ridge (Schlindwein, 2012) separates the Nansen and the Amundsen basins. Hydrothermal vents release trace metals (Edmonds et al., 2003) constantly (Baker et al., 2004). Additionally, sporadic explosive eruptions occur (Sohn et al., 2008); the biggest known such event was in 1999 at the 85°E volcanic complex (Schlindwein, 2012) and continued as earthquake swarms until 2001 (Schlindwein &

Riedel, 2010). Eruptive phases are rare but can last over decades (Schmid et al., 2017). Deep water circulation disperses hydrothermal plumes. Deep waters in the Nansen Basin flow cyclonically while the general circulation direction in the Amundsen Basin is westward (Figure 3) (Rudels, 2009). The only deep water pathway to the Atlantic Ocean is through Fram Strait, which has a less than 2,500 m sill depth.

Deep water in the central Nansen Basin has been reported to have lower particulate and higher dissolved ^{230}Th concentrations than over the slope region (Kirk Cochran et al., 1995). Residence times of ^{230}Th were reported to be 18–19 years in the central Nansen Basin and 10–12 years on the Barents Sea slope (Scholten et al., 1995). Almost 90% of the in situ produced ^{230}Th is estimated to be removed within the Arctic by scavenging (Moran et al., 2005).

We present dissolved, particulate, and total ^{230}Th and ^{232}Th results, as well as particulate ^{234}Th data, from expedition ARKXXIX/3 (GEOTRACES section GN04) conducted in 2015 and dissolved and total ^{230}Th data from expedition ARKXXII/2 (GIPY11) in 2007 and compare our results with those from 1991 (Scholten et al., 1995). We further investigate whether hydrothermal activity at the Gakkel Ridge leads to similar observations as in the Pacific and provide a new interpretation of how changes in this activity may affect trace element distributions in the Arctic Ocean. The first ^{230}Th time series allows us to assess the variability of hydrothermal scavenging over time.

2. Materials and Methods

2.1. Sampling and Analysis of Th in Samples Collected in 2007

Dissolved samples were filtered directly from the 24 L CTD-Niskin® bottles into cubitainers (LDPE) using 0.45-μm pore size Acropaks®. Samples were collected in volumes of 1, 2, and 10 L and acidified with concentrated ultraclean HNO$_3$. Seawater for the analysis of total ^{230}Th was sampled without filtration. The analyses were done at the University of Minnesota, Minneapolis, following methods described by Shen et al. (2003). The concentrations were measured using inductively coupled plasma-mass spectrometry (ICP-MS, Thermo Finnigan, Neptune) equipped with an secondary electron multiplier and a retarding potential quadrupole energy filter.

2.2. Sampling and Analysis of Th in Samples Collected in 2015

Analysis of ^{230}Th and ^{232}Th were performed in clean laboratories of the Alfred Wegener Institute, following GEOTRACES methods (Anderson et al., 2012). Water samples were filtered directly from the 24 L CTD-Niskin® bottles into cubitainers (LDPE) using 0.45-μm pore size Acropaks®. Seawater was sampled in volumes of 10 L (>2,000 m) and 20 L (<2,000 m), according to the expected concentrations (Nozaki et al., 1981).

Seawater samples were spiked with ^{229}Th and ^{236}U to prepare the isotope dilution analyses by ICP-MS. Spikes were calibrated against the reference standard material UREM11, a material in state of radioactive equilibrium (Hansen et al., 1983).

Particles were sampled using in situ pumps (McLane and Challenger Oceanic). Two hundred eight liters to 772 L of seawater were pumped through a 142 mm ø, 0.45 μm pore size Supor® (polyether sulfone) filter (Anderson et al., 2012). Filters were cut aboard for subsamples under a laminar flow hood on a cutting board using tweezers and scalpels. Approximately 5/6 of the filters were used for Thorium and ^{231}Pa (not shown in this study) analysis. A subsample (23 mm ø) was dried, placed onto plastic mounts, covered with Mylar and aluminum foil, and directly measured by beta decay counting of ^{234}Th ($t_{1/2}$ = 24.1 days) for at least 12 hr. Background measurements were performed 6 months later.

Filters were leached following the procedure described by Gdaniec et al. (2017). Filters were cut into pieces using ceramic scissors and placed into Teflon® beakers and then leached in 25–30 ml of 3 M HCl in ultrasonic baths). Samples were spiked with ^{233}Pa, ^{229}Th, and ^{236}U before leaching. After leaching, the sample solution was evaporated to less than 1 ml. Organic substances were dissolved by adding 8 M HNO$_3$ and H$_2$O$_2$ to the samples. Any remaining particles were separated by centrifugation and dissolved in concentrated HF. The two solutions were mixed and passed through anionic exchange columns following the protocol described in (Anderson et al., 2012). Measurements were performed using an ICP-MS (Thermo Scientific™ ELEMENT-2™) equipped with an Apex-Q (Elemental Scientific®).

3. Results

^{230}Th results are unsupported excess ^{230}Th (^{230}Th$_{xs}$); for simplification, here ^{230}Th refers to ^{230}Th$_{xs}$. Corrections were done following Hayes et al. (2015). The full radionuclide data set is available in the supporting information and at www.pangaea.de (https://doi.org/pangaea.de/10.1594/PANGAEA.893871).

3.1. Dissolved Th Concentrations

Both 2015 Nansen Basin profiles at stations 50 and 58 show a linear increase down to 2,000 m, followed by a sharp decrease below this depth (Figure 1a). Station 68/69 (2015) from the Gakkel Ridge shows a similar feature; high concentrations down to 1,500 m followed by a sharp decrease (Figure 1b). In 2015, dissolved ^{230}Th concentrations from the Amundsen Basin (station 81 and 117) increased linearly (Figure 1c) over the entire water column. Results from the Nansen Basin at station 260 (2007) show a similar profile compared to 2015, without a decrease below 2,000 m. Concentrations from three stations in the Makarov Basin in 2015 (shown as a scatter plot against dissolved iron (DFe) in Figure 2a) increased with depth and were much higher than in the Eurasian Basin (Figure 2a).

3.2. Particulate and Total Th Concentrations

Particulate ^{230}Th concentrations from 2015 are only available for station 50 (Figure 1d). At this station, up to 50% (3,000 m) of total ^{230}Th was particulate. The profile shows the highest values in the deep water (>2,000 m), reaching up to 6.5 fg/kg. Particulate ^{234}Th from 2015 (station 50) is shown as the relative amount of particulate ^{234}Th (Figure 1f), calculated from ^{238}U activities, assuming equilibrium of ^{234}Th with total ^{238}U in deep water (Owens et al., 2011). Between 2,600 and 3,500 m the particulate fraction is higher than above.

Total ^{230}Th concentrations (dissolved + particulate) decreased noticeably with depth in the Nansen Basin below 2,000 m in 2015 (Figure 1e). Station 260 (2007) shows a similar profile to 2015, without the decrease below 2,000 m. Total ^{232}Th at station 50 (2015) is lower and relatively constant below 2,000 m toward the ocean bottom (Figure 1g).

3.3. Changes in ^{230}Th Distributions Between 1991, 2007, and 2015

We compare data from 1991 (Scholten et al., 1995) with our 2007 and 2015 data (Figure 1a). Dissolved ^{230}Th concentrations in the Nansen Basin are generally lower in 2015 (stations 50 and 58) compared to 1991 and 2007. Only at 2,000 m depth at station 50 are dissolved ^{230}Th concentrations higher compared to samples from 1991 and 2007. The decrease in dissolved ^{230}Th concentrations in 2015 compared to 1991 and 2007 is most prominent below 2,000 m (Figure 1a).

Particulate ^{230}Th concentrations at station 50 (2015) were similar to those from station 239 (1991; Scholten et al., 1995; Figure 1d). Data from 2015 only exceed the 1991 data in the deepest samples (>3,000 m). Changes in total ^{230}Th in the Nansen Basin reveal almost the same pattern as dissolved ^{230}Th: Above 2,000 m values observed in 2007 and 2015 are similar to or lower than those from 1991. Values below 2,000 m from 2007 were in the range of the 1991 values. Values in 2015 were much lower (Figure 1e).

4. Discussion

4.1. Possible Reasons for Temporal Changes

Total ^{230}Th in the Nansen Basin below 2000 m decreased significantly after 2007 (Figure 1e). Advection could cause this decrease. We rule out advection from the Amundsen Basin as the reason, because dissolved ^{230}Th concentrations below 2,000 m in the Amundsen Basin are higher than at station 50 in the Nansen Basin. Moreover, deep waters in the Nansen Basin have lower CFC-11 concentrations than in the Amundsen Basin (Smethie, 2017). We exclude enhanced biological productivity because no significantly elevated net community production was found in the central Nansen Basin in 2011 (Ulfsbo et al., 2014). Scavenging removal induced by surface generated particles would evoke removal over the whole water column. We only observe depletion below 2,000 m.

Alternative particle sources are the Barents Sea shelf and slope. Sea ice formation in the Barents Sea produces dense waters (Rudels et al., 2000) that mix with the boundary current, collecting particles from slope sediments (Moran & Moore, 1991; Rudels et al., 2000). CFC-11 data show no evidence for shelf water cascading at station 50; in fact, values were even slightly lower compared to respective depths of surrounding
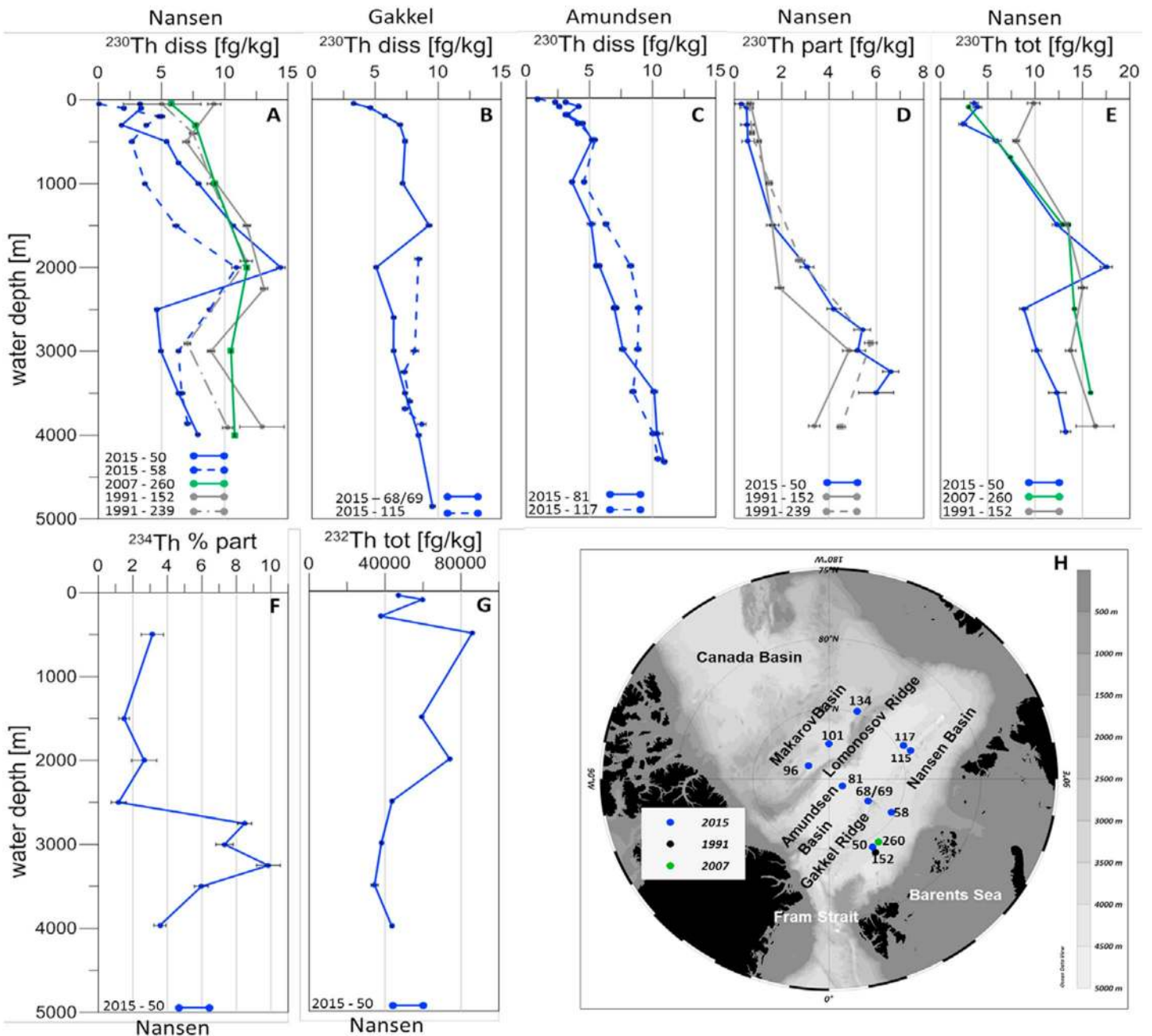
Figure 1. (a) Nansen Basin dissolved ^{230}Th concentrations from 1991, 2007 and 2015. (b) Gakkel Ridge dissolved ^{230}Th data from 2015. (c) Amundsen Basin dissolved ^{230}Th data from 2015. (d) Nansen Basin particulate ^{230}Th data from 1991 and 2015. (e) Total ^{230}Th data from 1991, 2007, and 2015. (f) Nansen Basin particulate ^{234}Th as a percentage of total ^{234}Th. (g) Total ^{232}Th data from 2015 (station 50). (h) Map of the location of the profiles shown in Figures 1a–1g; 1991 data are from Scholten et al. (1995).

stations (Smethie Jr., 2017). We also do not observe an enhancement in the fraction shelf/slope waters as indicated by radium isotopes. At 3,000 m, the ^{228}Ra/^{226}Ra activity ratio at station 50 was 0.017 ± 0.004 (Rutgers van der Loeff et al., 2018) and similar to prior measurements by Rutgers van der Loeff et al. (1995).

At station 50, the relative amount of particulate ^{234}Th and ^{230}Th below 2,000 m was higher than above (Figures 1d and 1f) indicating relatively high particle load at depth. Scholten et al. (1995) already reported elevated particulate ^{230}Th, interpreted, together with a slight decrease in dissolved ^{230}Th, as a consequence of periodically occurring nepheloid layers. This change did not affect total ^{230}Th (Scholten et al.,
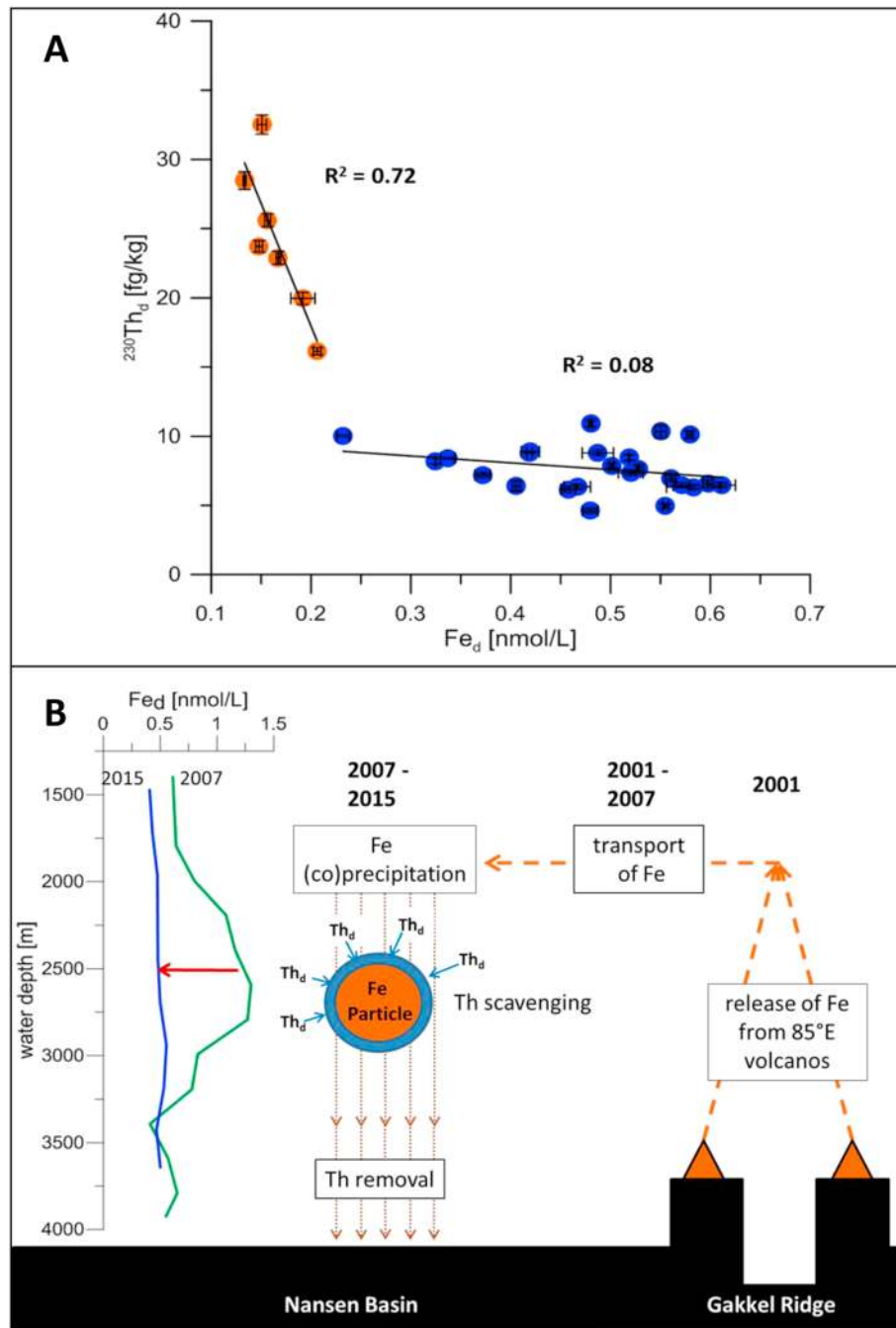
Figure 2. (a) Plot of dissolved ^{230}Th against dissolved iron from Rijkenberg et al. (2018) below 2,000 m. Eurasian Basin is blue, and Makarov Basin is orange. Quality of relationships is given R^2 values. (b) Conceptual model of hydrothermal removal process: Fe is released by the vents (Edmonds et al., 2003) and stabilized as dissolved or dissolved and microparticles, which allow it to circulate around the Nansen Basin. Later, oxidation forms Fe oxy-hydroxide particles or Fe reacts with particles being there, which scavenge and remove Th. (left) Dissolved iron from stations 50 (2015, blue) and 260 (2007, green) (Klunder et al., 2012).

1995). We explain the difference in depth distribution of particulate ^{230}Th and particulate ^{234}Th as a result of the different time scales controlling these signals: Changes in particle load will be reflected in changes in particulate ^{234}Th on the time scale of ^{234}Th decay, whereas the distribution of particulate ^{230}Th will adjust on the much longer time scale of the scavenging coefficient. The difference in depth distribution between particulate ^{234}Th and particulate ^{230}Th therefore illustrates the temporal variability of particle loads, for example, due to periodically occurring nepheloid layers. We conclude that a lateral supply of

suspended particles at depth does play a role in Th scavenging in the Nansen Basin but we see no evidence for an increase of resuspended particles since 1991, given the similar ^{228}Ra/^{226}Ra activity ratios in 1991 and 2015 and the findings of Scholten et al. (1995) that periodically occurring nepheloid layers do not reduce total ^{230}Th.

Dissolved ^{230}Th concentrations in the Makarov Basin are much higher than in the Nansen Basin, which implies a low scavenging regime in the Makarov Basin due to low particle inputs in addition to long water mass residence time (Scholten et al., 1995). In 2007, Klunder et al. (2012) observed that DFe was lower in the Makarov Basin than in the Eurasian Basin and explained this by the absence of Fe sources that affect the Nansen Basin. Low concentrations of DFe coincide with high concentrations of dissolved ^{230}Th in the Makarov Basin (Figure 2a), while DFe in the deep Nansen Basin is generally higher and ^{230}Th lower. This shows two different scavenging regimes in the Eurasian Basin and Makarov Basin. The higher inputs of DFe in the Eurasian Basin enhance Fe oxy-hydroxide production and subsequent scavenging of particle reactive elements. We cannot conclude that the two scavenging regimes are only due to the presence or absence of hydrothermal vents, but we argue that the difference is controlled by DFe inputs. Therefore any additional Fe input would change the scavenging situation.

Continuous hydrothermal venting at the Gakkel Ridge (Baker et al., 2004; Edmonds et al., 2003; Michael et al., 2003) is reflected by a small DFe containing hydrothermal plume at station 68/69 (Gakkel Ridge) in 2015 in the immediate vicinity of a known vent (Rijkenberg et al., 2018). Hence, we assume that continuous venting is part of the background steady state situation as observed in 1991. We interpret the decrease at depth in ^{230}Th at Station 68/69 as a consequence of scavenging by this steady venting. This decrease fits to observations from the East Pacific Rise (Pavia et al., 2017). Since DFe was much higher in 2007 and dispersed over a larger area than in 2015 we conclude that the 2007 plume must have had another source than permanent venting and we hypothesize that it was caused by explosive volcanic eruptions at the Gakkel Ridge (Sohn et al., 2008).

^{230}Th decreased below 2,000 m at station 50, consistent with the plume depth from the eruptions in 2001 (Baker et al., 2004; Stranne et al., 2010). These eruptions release large amounts of material (Sohn et al., 2008) and can cause "mega plumes" (Cann & Strens, 1989; Clague et al., 2009). Hence, explosive eruptions may overprint the steady state situation.

4.2. Hypothesis of Transient Scavenging by Eruptional Hydrothermal Fe

Elevated DFe concentrations at discrete depth horizons in the Eurasian Basin in 2007 with highest concentrations at the Gakkel Ridge and in the south western Nansen Basin in 2,000–3,500 m were described as a hydrothermal plume from continuous venting (Klunder et al., 2012; Middag et al., 2011). Based on our ^{230}Th time series and new DFe from 2015 we interpret the high DFe data from 2007 as a plume released by huge eruptions. That means that after dispersal of the eruptive plume the scavenging regime in the Nansen Basin was no longer in a steady state.

After 2007 until 2015, when only much smaller Fe peaks were observed and ^{230}Th decreased below 2,000 m, a scavenging event must have taken place.

We hypothesize that formation of Fe oxy-hydroxides by, for example, precipitation or coprecipitation caused by the Fe input increased particle concentration and changed their composition. Therefore, we think that DFe removal triggered ^{230}Th scavenging. Between 2007 and 2015 scavenging of ^{230}Th occurred and resulted in DFe and ^{230}Th removal by 2015. Figure 2b shows a conceptual model about this process.

The negative imprint of removed ^{230}Th persists for many years, as production from ^{234}U and supply from above 2,000 m is only 2.34 fg/kg in 4 years (half the time between 2007 and 2015), following the approach of Pavia et al. (2017) and using the difference in ^{230}Th flux into and out of the plume (2,000–3,990 m) and a settling rate from Rutgers van der Loeff et al. (2018).

By 2015 the additional eruptive Fe has been removed together with parts of dissolved ^{230}Th. Particulate ^{230}Th in 2015 is similar to 1991, while total and dissolved ^{230}Th are significantly lower now. The extreme DFe peaks vanished but DFe is still higher in the Nansen Basin than in Makarov Basin. Our Nansen Basin ^{230}Th profile from 2007 suggests that any additional scavenging caused by removal of eruptive Fe had not yet caused ^{230}Th removal by 2007.

While measurements of particulate iron (PFe) and other potential scavengers in the plume are not available, we can estimate their contribution to adsorption of ^{230}Th from analogies to the South East Pacific (GEOTRACES Section GP16), based on the observed distribution of DFe in the Arctic in 2007 and 2015. To this end we establish a PFe/DFe ratio within and outside the plume in the Pacific and apply this to the Arctic. With this estimate of PFe in the Arctic, we use published estimates of distribution coefficients for Th in the presence of natural Fe $(OH)_3$ to determine the possible contribution of PFe to ^{230}Th scavenging. DFe data from the Arctic are quite comparable to GP 16 in the distant plume: For 2007, Klunder et al. (2012) report ~1.25 nmol/L, similar to the Pacific plume (Fitzsimmons et al., 2014). For 2015, 0.5 nmol/L is reported, similar to background concentration at the depth of the plume at GP16. PFe/DFe ratios at GP16 range from unity to three, both at the distant plume sites and for the background below 2,500 m (Fitzsimmons et al., 2014; Lam et al., 2018). This results in an estimated PFe concentration in the deep Nansen Basin of 1.25–3.75 nM (2007) and 0.5–1.5 nM (2015) corresponding to Fe $(OH)_3$ concentrations of 134–402 ng/L PFe for 1.25 nM DFe (2007) or 53.5–160.5 ng/L PFe for 0.5 nM DFe (2015). We now apply the K_d value of ^{230}Th for Fe $(OH)_3$ from Hayes et al. (2015) of $32.8*10^7$ and learn that 4.4–13.2% of ^{230}Th in 2007 (1.75–5.25% in 2015) would be expected to be found on particles in the Arctic, solely due to PFe.

In 2007, about 25% of ^{230}Th is particulate (based on the difference of total and dissolved ^{230}Th from alternating depths), which means that the above estimate (up to 13.2% of ^{230}Th on the Fe $(OH)_3$ phase) explains up to half of particulate ^{230}Th. In 2015, the high fraction of particulate Th isotopes, up to 50% particulate ^{230}Th at the plume depth, indicates the presence of a suspended particulate phase with either high mass concentrations or with a very high K_d. The high percentage particulate ^{230}Th cannot be explained by Fe $(OH)_3$ scavenging using the analogy to GP16. In this year, hydrothermal Fe $(OH)_3$ can only explain a small fraction of ^{230}Th removal and the precise mechanisms that have led to the situation observed in 2015 remain unclear and require further investigation of other potential scavengers, for example, MnO_2.

4.3. Plume Dispersal

We have argued above that the hydrothermal scavenging in the Nansen Basin is not in steady state but temporally enhanced by a plume released by eruptive volcanism. We discuss here how we think that this plume has dispersed and circulated in the deep basins. Klunder et al. (2012) reported a vent at 37°E or a plume from probably 85°E as a possible plume source. Klunder et al. (2012) and Middag et al. (2011) explained the horizontal dispersion of the plume as a combination of eddy diffusion and scavenging removal following the 1-dimensional first-order scavenging model of Weiss (1977). Their best fit was achieved using 5–15 years scavenging residence time for Fe (Klunder et al., 2012) and 0.4–2 years for Mn (Middag et al., 2011) on the basis of the horizontal eddy diffusion coefficient $K_h = 5 \times 10^6$ cm^2/s (Weiss, 1977). They explained the much longer residence time of Fe compared to Mn by Fe complexation with organic ligands (Thuróczy et al., 2011). Their models show that the basin wide dispersal could be due to horizontal diffusion from a single source over many years, although deep water circulation and multiple plume sources (Baker et al., 2004; Edmonds et al., 2003) complicate their calculations. They assumed a steady state distribution and based their calculations on the model of Weiss (1977), developed to describe the Mn field around a constant vent. Our new ^{230}Th data are in conflict with a scavenging process at steady state.

4.4. Plume Dispersal by Deep Water Circulation

Until 2015, the eruptive plume affected water masses must have spread over larger areas of the Nansen Basin by eddy diffusion and (re) circulation within the basin. We interpret our 2015 data from station 50 and 58 as fully affected by the plume. Figure 2b shows a theoretical concept of how plume intensity and subsequent scavenging can differ between Amundsen and Nansen basins due to circulation. Fe from eruptions in 2001 was dispersed, by the deep water circulation (Figure 3). There might be recirculation (white dashed arrows in Figure 3) within the Nansen Basin that retains hydrothermally influenced water masses in this basin (yellow dashed oval in Figure 3). Plume signals in the Amundsen Basin in 2007 could be due to eddy diffusion, smaller plume branches, or both, and could have given rise to some hydrothermal scavenging. But the major part of the plume in the Amundsen Basin is expected to be transported out of the basin toward Fram Strait (Figure 3). Therefore, ^{230}Th profiles from the Amundsen Basin do not represent hydrothermal scavenging as those from the Nansen Basin (Figure 1b).
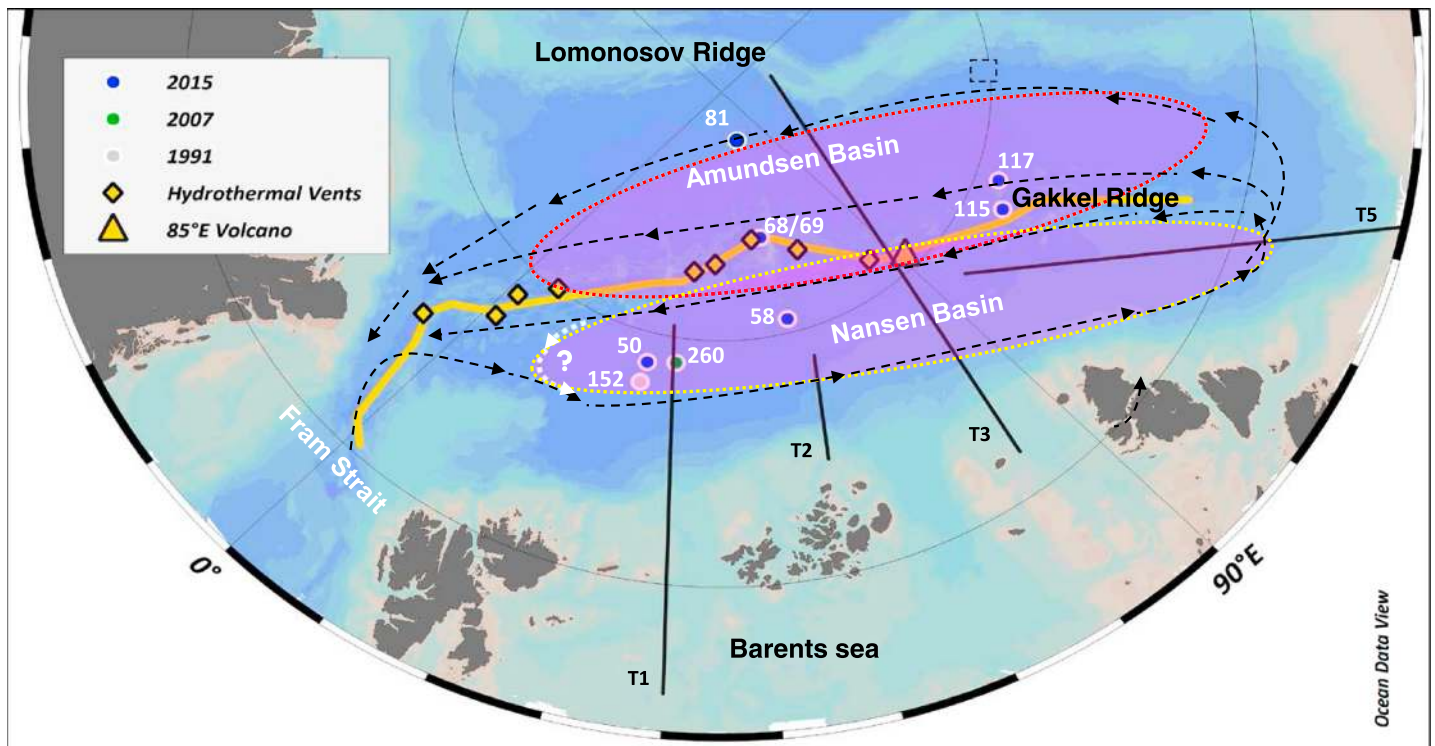
Figure 3. Model of plume dispersal and Eurasian Basin deep water circulation (black dashed lines; Rudels, 2009) including potential recirculation (white dashed line). Locations of stations from 2015, 2007, and 1991 are indicated with colored dots (see legend). Solid black lines are transects where in 2007 elevated Fe concentrations were observed (Klunder et al., 2012). Two plume circulation pathways are presented: The yellow dashed line represents a plume circulation confined to the Nansen Basin, and the red dashed line shows a plume dispersal to the Amundsen Basin where the plume is removed faster by circulation. Map was created using Ocean Data View (Schlitzer, 2016).

5. Conclusions

We provide evidence in support of hydrothermal activity as a potential trigger mechanism for scavenging of particle reactive elements in the Nansen Basin. Specifically, ^{230}Th activities below 2,000 m have changed between 2007 and 2015 as a result of a scavenging event, interpreted as hydrothermally induced. The ^{230}Th time series suggests that Th scavenging in the Nansen Basin is not in steady state following submarine volcanic eruptions. The mechanism explaining the dispersal of the hydrothermal plume throughout the Nansen Basin will require further investigation, as well as the precise mechanism of eruptive Fe cycling leading to the 2015 situation. This proposed role of episodic hydrothermal input provides new insights on the nature of hydrothermal scavenging in the Arctic and how other trace elements may be removed from the Arctic. Submarine volcanic eruptions may also influence the distribution of other trace elements in the Nansen Basin, perhaps more than in other oceans, due to the small size and enclosed nature of the Eurasian Basins. The concurrence of geochemical and geophysical data may also improve interpretations of other trace element distributions from the Eurasian Arctic Ocean. Time variable signals, as seen in ^{230}Th and DFe, complicate the interpretation of tracer data in the Arctic as being at steady state and show the value of repeated GEOTRACES occupations in understanding variability of scavenging processes in the deep ocean.

References

Anderson, R. F., Fleisher, M. Q., Robinson, L., Edwards, R. L., Hoff, J. A., Moran, S. B., et al. (2012). GEOTRACES intercalibration of ^{230}Th, ^{232}Th, ^{231}Pa, and prospects for ^{10}Be. *Limnology and Oceanography: Methods*, *10*(4), 179–213. https://doi.org/10.4319/lom.2012.10.179

Bacon, M. P., & Anderson, R. F. (1982). Distribution of thorium isotopes between dissolved and particulate forms in the deep sea. *Journal of Geophysical Research*, *87*(C3), 2045–2056. https://doi.org/10.1029/JC087iC03p02045

Baker, E. T., Edmonds, H. N., Michael, P. J., Bach, W., Dick, H. J. B., Snow, J. E., et al. (2004). Hydrothermal venting in magma deserts: The ultraslow-spreading Gakkel and Southwest Indian ridges. *Geochemistry, Geophysics, Geosystems*, *5*, Q08002. https://doi.org/10.1029/2004GC000712

Cann, J. R., & Strens, M. R. (1989). Modeling periodic megaplume emission by black smoker systems. *Journal of Geophysical Research*, *94*(B9), 12,227–12,237. https://doi.org/10.1029/JB094iB09p12227

Clague, D. A., Paduan, J. B., & Davis, A. S. (2009). Widespread strombolian eruptions of mid-ocean ridge basalt. *Journal of Volcanology and Geothermal Research*, *180*(2-4), 171–188. https://doi.org/10.1016/j.jvolgeores.2008.08.007

Coppola, L., Roy-Barman, M., Mulsow, S., Povinec, P., & Jeandel, C. (2006). Thorium isotopes as tracers of particles dynamics and deep water circulation in the Indian sector of the Southern Ocean (ANTARES IV). *Marine Chemistry*, *100*(3-4), 299–313. https://doi.org/10.1016/j.marchem.2005.10.019

Edmonds, H. N., Michael, P. J., Baker, E. T., Connelly, D. P., Snow, J. E., Langmuir, C. H., et al. (2003). Discovery of abundant hydrothermal venting on the ultraslow-spreading Gakkel ridge in the Arctic Ocean. *Nature*, *421*(6920), 252–256. https://doi.org/10.1038/nature01351

Fitzsimmons, J. N., Boyle, E. A., & Jenkins, W. J. (2014). Distal transport of dissolved hydrothermal iron in the deep South Pacific Ocean. *Proceedings of the National Academy of Sciences*, *111*(47), 16,654–16,661. https://doi.org/10.1073/pnas.1418778111

Gdaniec, S., Roy-Barman, M., Foliot, L., Thil, F., Dapoigny, A., Burckel, P., et al. (2017). Thorium and protactinium isotopes as tracers of marine particle fluxes and deep water circulation in the Mediterranean Sea. *Marine Chemistry*, *199*, 12–23.

German, C. R., Colley, S., Palmer, M. R., Khripounoff, A., & Klinkhammer, G. P. (2002). Hydrothermal plume-particle fluxes at 13°N on the East Pacific Rise. *Deep Sea Research Part I: Oceanographic Research Papers*, *49*(11), 1921–1940. https://doi.org/10.1016/S0967-0637(02)00086-9

German, C. R., Fleer, A. P., Bacon, M. P., & Edmond, J. M. (1991). Hydrothermal scavenging at the Mid-Atlantic Ridge: Radionuclide distributions. *Earth and Planetary Science Letters*, *105*(1-3), 170–181. https://doi.org/10.1016/0012-821X(91)90128-5

Hansen, R. G., Ring, E. J., T. Council for Mineral, & D. Analytical Chemistry (1983). *The preparation and certification of a uranium reference material*. Randburg, South Africa: Council for Mineral Technology.

Hayes, C. T., Anderson, R. F., Fleisher, M. Q., Vivancos, S. M., Lam, P. J., Ohnemus, D. C., et al. (2015). Intensity of Th and Pa scavenging partitioned by particle chemistry in the North Atlantic Ocean. *Marine Chemistry*, *170*, 49–60. https://doi.org/10.1016/j.marchem.2015.01.006

Henderson, G. M., Heinze, C., Anderson, R. F., & Winguth, A. M. E. (1999). Global distribution of the ^{230}Th flux to ocean sediments constrained by GCM modelling. *Deep Sea Research, Part I*, *46*, 1861–1893.

Kirk Cochran, J., Hirschberg, D. J., Livingston, H. D., Buesseler, K. O., & Key, R. M. (1995). Natural and anthropogenic radionuclide distributions in the Nansen Basin, Artic Ocean: Scavenging rates and circulation timescales. *Deep Sea Research, Part II*, *42*, 1495–1517.

Klinkhammer, G., Bender, M., & Weiss, R. F. (1977). Hydrothermal manganese in the Galapagos rift. *Nature*, *269*(5626), 319–320. https://doi.org/10.1038/269319a0

Klunder, M. B., Laan, P., Middag, R., de Baar, H. J. W., & Bakker, K. (2012). Dissolved iron in the Arctic Ocean: Important role of hydrothermal sources, shelf input and scavenging removal. *Journal of Geophysical Research*, *117*, C04014. https://doi.org/10.1029/2011JC007135

Lam, P. J., Lee, J.-M., Heller, M. I., Mehic, S., Xiang, Y., & Bates, N. R. (2018). Size-fractionated distributions of suspended particle concentration and major phase composition from the U.S. GEOTRACES Eastern Pacific Zonal Transect (GP16). *Marine Chemistry*, *201*, 90–107. https://doi.org/10.1016/j.marchem.2017.08.013

Michael, P. J., Langmuir, C. H., Dick, H. J. B., Snow, J. E., Goldstein, S. L., Graham, D. W., et al. (2003). Magmatic and amagmatic seafloor generation at the ultraslow-spreading Gakkel ridge, Arctic Ocean. *Nature*, *423*(6943), 956–961. https://doi.org/10.1038/nature01704

Middag, R., de Baar, H. J. W., Laan, P., & Klunder, M. B. (2011). Fluvial and hydrothermal input of manganese into the Arctic Ocean. *Geochimica et Cosmochimica Acta*, *75*(9), 2393–2408. https://doi.org/10.1016/j.gca.2011.02.011

Moran, S. B., & Moore, R. M. (1991). The potential source of dissolved aluminum from resuspended sediments to the North Atlantic Deep Water. *Geochimica et Cosmochimica Acta*, *55*(10), 2745–2751. https://doi.org/10.1016/0016-7037(91)90441-7

Moran, S. B., Shen, C.-C., Edwards, R. L., Edmonds, H. N., Scholten, J. C., Smith, J. N., & Ku, T.-L. (2005). ^{231}Pa and ^{230}Th in surface sediments of the Arctic Ocean: Implications for ^{231}Pa/^{230}Th fractionation, boundary scavenging, and advective export. *Earth and Planetary Science Letters*, *234*, 235–248.

Nozaki, Y., Horibe, Y., & Tsubota, H. (1981). The water column distributions of thorium isotopes in the western North Pacific. *Earth and Planetary Science Letters*, *54*(2), 203–216. https://doi.org/10.1016/0012-821X(81)90004-2

Owens, S. A., Buesseler, K. O., & Sims, K. W. W. (2011). Re-evaluating the ^{238}U-salinity relationship in seawater: Implications for the ^{238}U–^{234}Th disequilibrium method. *Marine Chemistry*, *127*(1-4), 31–39. https://doi.org/10.1016/j.marchem.2011.07.005

Pavia, F., Anderson, R., Vivancos, S., Fleisher, M., Lam, P., Lu, Y., et al. (2017). Intense hydrothermal scavenging of ^{230}Th and ^{231}Pa in the deep Southeast Pacific. *Marine Chemistry*, *201*, 212–228.

Resing, J. A., Sedwick, P. N., German, C. R., Jenkins, W. J., Moffett, J. W., Sohst, B. M., & Tagliabue, A. (2015). Basin-scale transport of hydrothermal dissolved metals across the South Pacific Ocean. *Nature*, *523*(7559), 200–203. https://doi.org/10.1038/nature14577

Rijkenberg, M. J. A., Slagter, H. A., Rutgers van der Loeff, M., van Ooijen, J., & Gerringa, L. J. A. (2018). Dissolved Fe in the deep and upper Arctic Ocean with a focus on Fe limitation in the Nansen Basin. *Frontiers in Marine Science*, *5*(88). https://doi.org/10.3389/fmars.2018.00088

Roy-Barman, M., Coppola, L., & Souhaut, M. (2002). Thorium isotopes in the western Mediterranean Sea: An insight into the marine particle dynamics. *Earth and Planetary Science Letters*, *196*(3-4), 161–174. https://doi.org/10.1016/S0012-821X(01)00606-9

Rudels, B. (2009). Arctic Ocean circulation A2—Steele, John H. In *Encyclopedia of ocean sciences* (2nd ed., pp. 211–225). Oxford: Academic Press.

Rudels, B., Muench, R. D., Gunn, J., Schauer, U., & Friedrich, H. J. (2000). Evolution of the Arctic Ocean boundary current north of the Siberian shelves. *Journal of Marine Systems*, *25*(1), 77–99. https://doi.org/10.1016/S0924-7963(00)00009-9

Rutgers van der Loeff, M. M., Key, R. M., Scholten, J., Bauch, D., & Michel, A. (1995). 228Ra as a tracer for shelf water in the Arctic Ocean. *Deep Sea Research, Part II*, *42*(6), 1533–1553. https://doi.org/10.1016/0967-0645(95)00053-4

Rutgers van der Loeff, M. M., Kipp, L., Charette, M. A., Moore, W. S., Black, E., Stimac, I., et al. (2018). Radium isotopes across the Arctic Ocean show time scales of water mass ventilation and increasing shelf inputs. *Journal of Geophysical Research: Oceans*, *123*, 4853–4873. https://doi.org/10.1029/2018JC013888

Saito, M. A., Noble, A. E., Tagliabue, A., Goepfert, T. J., Lamborg, C. H., & Jenkins, W. J. (2013). Slow-spreading submarine ridges in the South Atlantic as a significant oceanic iron source. *Nature Geoscience*, *6*, 775–779.

Santschi, P. H., Murray, J. W., Baskaran, M., Benitez-Nelson, C. R., Guo, L. D., Hung, C.-C., et al. (2006). Thorium speciation in seawater. *Marine Chemistry*, *100*(3-4), 250–268. https://doi.org/10.1016/j.marchem.2005.10.024

Schlindwein, V. (2012). Teleseismic earthquake swarms at ultraslow spreading ridges: Indicator for dyke intrusions? *Geophysical Journal International*, *190*(1), 442–456. https://doi.org/10.1111/j.1365-246X.2012.05502.x

Schlindwein, V., & Riedel, C. (2010). Location and source mechanism of sound signals at Gakkel ridge, Arctic Ocean: Submarine Strombolian activity in the 1999–2001 volcanic episode. *Geochemistry, Geophysics, Geosystems*, *11*, Q01002. https://doi.org/10.1029/2009GC002706

Schlitzer, R. (2016). Ocean Data View, edited, http://odv.awi.de.

Schmid, F., Schlindwein, V., Koulakov, I., Plötz, A., & Scholz, J.-R. (2017). Magma plumbing system and seismicity of an active mid-ocean ridge volcano, 7, 42949.

Scholten, J. C., Rutgers van der Loeff, M. M., & Michel, A. (1995). Distribution of ^{230}Th and ^{231}Pa in the water column in relation to the ventilation of the deep Arctic basins. *Deep Sea Research, Part II, 42*, 1519–1531.

Shen, C.-C., Cheng, H., Edwards, R. L., Moran, S. B., Edmonds, H. N., Hoff, J. A., & Thomas, R. B. (2003). Measurement of attogram quantities of ^{231}Pa in dissolved and particulate fractions of seawater by isotope dilution thermal ionization mass spectroscopy. *Analytical Chemistry, 75*(5), 1075–1079. https://doi.org/10.1021/ac026247r

Smethie, W. M., Jr. (2017). CFC-11, CFC-12, CFC-113, and SF6 measured on water bottle samples during POLARSTERN cruise PS94 (ARK-XXIX/3) to the Arctic Ocean in 2016, edited, PANGAEA.

Sohn, R. A., Willis, C., Humphris, S., Shank, T. M., Singh, H., Edmonds, H. N., et al. (2008). Explosive volcanism on the ultraslow-spreading Gakkel ridge, Arctic Ocean. *Nature, 453*(7199), 1236–1238. https://doi.org/10.1038/nature07075

Stranne, C., Sohn, R. A., Liljebladh, B., & Nakamura, K.-I. (2010). Analysis and modeling of hydrothermal plume data acquired from the 85°E segment of the Gakkel Ridge. *Journal of Geophysical Research, 115*, C06028. https://doi.org/10.1029/2009JC005776

Thuróczy, C. E., Gerringa, L. J. A., Klunder, M., Laan, P., Le Guitton, M., & de Baar, H. J. W. (2011). Distinct trends in the speciation of iron between the shallow shelf seas and the deep basins of the Arctic Ocean. *Journal of Geophysical Research, 116*, C10009. https://doi.org/10.1029/2010JC006835

Ulfsbo, A., Cassar, N., Korhonen, M., van Heuven, S., Hoppema, M., Kattner, G., & Anderson, L. G. (2014). Late summer net community production in the central Arctic Ocean using multiple approaches. *Global Biogeochemical Cycles, 28*, 1129–1148. https://doi.org/10.1002/2014GB004833

Weiss, R. F. (1977). Hydrothermal manganese in the deep sea: Scavenging residence time and Mn/3He relationships. *Earth and Planetary Science Letters, 37*(2), 257–262. https://doi.org/10.1016/0012-821X(77)90171-6